electronics

MDPI

Article

Simulating Quantum Pauli Noise with Three Independently Controlled Pauli Gates

François Chapeau-Blondeau

Laboratoire Angevin de Recherche en Ingénierie des Systèmes (LARIS), Université d'Angers, 62 Avenue Notre Dame du Lac, 49000 Angers, France; f.chapeau@univ-angers.fr

Abstract: A quantum Pauli noise is a nonunitary process that alters the state of a qubit by random application of the four Pauli operators. We investigate a four-qubit quantum circuit, consisting of a pipeline of three independently controlled Pauli gates, for simulating the general class of qubit Pauli noises. The circuit with a fixed architecture is controllable by three separable quantum states from three auxiliary qubits in order to adjust the parameters of the targeted Pauli noise on the principal qubit. Important Pauli noises such as bit flip, phase flip, bit phase flip, and depolarizing noise are readily simulated, along with an infinite subset of other Pauli noises. However, the quantum circuit with its simple and fixed architecture cannot simulate all conceivable Pauli noises, and a characterization is proposed, in the parameter space of the Pauli noises, denoting those that are simulable by the circuit and those that are not. The circuit is a useful tool to contribute to controlled simulation, on current or future quantum processors, of nonunitary processes of noise and decoherence.

Keywords: quantum noise; quantum circuit; Pauli gates; quantum simulation; quantum signal

1. Introduction

Quantum technologies, present and forthcoming, have to operate, in realistic practical conditions, in the presence of quantum noise or decoherence [1–3]. Accordingly, quantum noise or decoherence represents a major factor for the operation and development of quantum technologies. It is therefore crucial to take quantum noise into account when designing and evaluating quantum methodologies and devices for quantum signal and information processing.

Significant efforts are being made to reduce or mitigate quantum noise in the physical implementation of quantum devices as much as is feasible. An inevitable residual amount of noise is nevertheless realistic to envisage in this sector, and, from a broader perspective, quantum noise or decoherence may result from an imposed environment and the given external conditions where the quantum devices have to operate. It is therefore broadly relevant to tailor and optimize the quantum signals, information processing, and devices to efficiently cope with noise. Many areas and tasks of quantum technologies are concerned with this perspective, such as the following examples.

For communication over a quantum channel, efficient signaling and encoding at the input, efficient measurement and decoding at the output, the performance of quantum error correcting codes, and the information capacities and their approaching or achieving conditions all generally depend on the quantum noise over the channel [4,5]. The performances of cryptosystems, cryptographic protocols, encryption and decryption, and quantum key distribution generally depend on the quantum noise present [6,7]. For quantum sensors and metrology, the input quantum signals used for probing, their measurement and processing at the output, and the quantum protocols in use for parameter estimation and for state or process tomography all generally need to be designed and optimized according to the noise conditions [8–10]. Quantum control, quantum optimization, quantum annealing, and quantum machine learning can also have their performance affected by noise [11–14]

Citation: Chapeau-Blondeau, F. Simulating Quantum Pauli Noise with Three Independently Controlled Pauli Gates. *Electronics* **2024**, *13*, 439. https://doi.org/10.3390/electronics13020439

Academic Editor: Wiesław Leonski

Received: 13 December 2023
Revised: 17 January 2024
Accepted: 19 January 2024
Published: 21 January 2024

and may require optimization for optimal efficiency, for instance to exploit a controlled level of noise to escape local suboptimal solutions, or to exploit more special noise effects such as stochastic resonance [15–17]. Fault-tolerant quantum computation is also directly concerned with the influence of quantum noise [18,19].

All these areas and tasks, for the design and optimization of the quantum signals, quantum processing, and quantum devices involved, may benefit from experimental testbeds where quantum noise is applicable in controlled conditions so as to assess its impact in various scenarios. Such controlled simulation of quantum noise can be obtained by means of appropriate noise models implemented on quantum circuits accessible from current or future quantum processors. In this respect, various circuit models are accessible to simulate important quantum noises, especially with relevance to the qubit [20,21], which is a fundamental object of quantum information, yet not exhaustively covering all conceivable qubit noises. Also, different circuit models are possible depending on the constraints imposed on the circuit hardware, but no systematic methodology yet exists to derive and optimize the models, even for the essential case of qubit noises.

To contribute in this direction of controlled simulation of quantum noises, in this article, we address the important class of quantum Pauli noises on a qubit. We will consider a quantum circuit with a simple fixed pipeline architecture of three controlled standard quantum gates. Moreover, we will investigate the capability of this quantum circuit in order to simulate Pauli noises over a broad (infinite) range of instances while enabling easy control regarding the noise parameters.

2. Quantum Pauli Noise

A general Pauli noise [4] is a nonunitary process that alters the quantum state ρ of a qubit through random application of the four Pauli operators $\{\sigma_0 \equiv \mathrm{I}_2, \sigma_x, \sigma_y, \sigma_z\}$, which form an orthogonal basis for operators on the two-dimensional qubit Hilbert space $\mathcal{H}_2$. Accordingly, the action of such a Pauli noise on a density operator ρ can be represented by the quantum operation with the operator-sum representation

$$\rho \longmapsto \mathcal{N}(\rho) = \sum_{k=0,x,y,z} p_k \sigma_k \rho \sigma_k^\dagger \,, \tag{1}$$

with (p_0, p_x, p_y, p_z), a probability distribution satisfying the normalization condition $p_0 + p_x + p_y + p_z = 1$, and the four Kraus operators $\Lambda_k = \sqrt{p_k}\sigma_k$. Pauli noises form a useful class of quantum noise that has been considered in many contexts of application, for instance for detection [22] or estimation [23–25] with quantum signals, or for investigating specific properties of quantum noises [26,27]. The class of Pauli noises of Equation (1) in particular contains important noises [20] such as the bit-flip noise when $(p_0, p_x, p_y, p_z) = (1 - p_x, p_x, 0, 0)$, the phase-flip noise when $(p_0, p_x, p_y, p_z) = (1 - p_z, 0, 0, p_z)$, the bit-phase-flip noise when $(p_0, p_x, p_y, p_z) = (1 - p_y, 0, p_y, 0)$, and the depolarizing noise when $(p_0, p_x, p_y, p_z) = (1 - p, p/3, p/3, p/3)$ parametrized by the probability $p = 1 - p_0$.

Equivalently, on a qubit density operator $\rho = \left(\mathrm{I}_2 + \vec{r} \cdot \vec{\sigma}\right)/2$ in standard Bloch representation [20], the quantum operation of Equation (1) realizes in $\mathbb{R}^3$ the transformation of the Bloch vector

$$\vec{r} \longmapsto \vec{r}\,' = \begin{bmatrix} a_x & 0 & 0 \\ 0 & a_y & 0 \\ 0 & 0 & a_z \end{bmatrix} \vec{r} \,, \tag{2}$$

with the three real scalar matrix elements

$$\begin{cases} a_x = p_0 + p_x - p_y - p_z = 1 - 2(p_y + p_z) \,, & (3) \\ a_y = p_0 - p_x + p_y - p_z = 1 - 2(p_x + p_z) \,, & (4) \\ a_z = p_0 - p_x - p_y + p_z = 1 - 2(p_x + p_y) \,. & (5) \end{cases}$$

The three parameters a_k in Equations (3)–(5) are contraction factors satisfying $0 \leq |a_k| \leq 1$ for all $k \in \{x, y, z\}$, to guarantee that the Bloch ball of valid Bloch vectors is mapped into

itself. The transformation of Equation (2) by noise contracts the Bloch vectors in a generally nonuniform way along the three directions, Ox, Oy, and Oz, of $\mathbb{R}^3$. An increasing level of noise corresponds to a more pronounced contraction. The maximum level of contraction would occur as $a_x = a_y = a_z = 0$, corresponding to a noisy state with a null Bloch vector $\vec{0}$ characterizing the maximally mixed qubit state $\mathrm{I}_2/2$ identifiable with the maximally noisy state.

Alternatively, the nonunitary quantum operation $\mathcal{N}(\cdot)$ defined in Equation (1) by an operator-sum representation can be described through an interaction with an (unobserved) environment in the form of a Stinespring dilated unitary representation [20]. For a principal quantum system Q initially with the density operator ρ, the environment E is initially prepared in a pure state $|e_0\rangle$, and a joint unitary operator U_{QE} is introduced [20] to describe the evolution of the system-environment compound QE generically occurring as $\rho \otimes |e_0\rangle \langle e_0| \mapsto \mathsf{U}_{QE}(\rho \otimes |e_0\rangle \langle e_0|)\mathsf{U}_{QE}^{\dagger}$. Finally, after this joint unitary evolution, the final state of the principal system Q is obtained by partial tracing over the environment E as

$$\mathrm{tr}_E\left[\mathsf{U}_{QE}(\rho \otimes |e_0\rangle \langle e_0|)\mathsf{U}_{QE}^{\dagger}\right] = \mathcal{N}(\rho)\ . \tag{6}$$

The constitutive details of the environment are largely wiped off in the partial trace operation of Equation (6), and an infinite set of environment models (isometrically related) equivalently lead to the same evolution $\rho \mapsto \mathcal{N}(\rho)$ from Equation (6) for the principal system Q. For a quantum noise on Q, a simulator enabling control of the noise properties can be constructed as a quantum system offering an adequate model for the environment. The environment model has to be designed, via the choice of $|e_0\rangle$ and U_{QE}, so as to match in Equation (6) the quantum operation $\mathcal{N}(\cdot)$ defined by the operator-sum representation of Equation (1).

For a quantum operation $\rho \mapsto \mathcal{N}(\rho) = \sum_{k=1}^{K} \Lambda_k \rho \Lambda_k^{\dagger}$ defined by K Kraus operators Λ_k, one possibility can be to select a K-dimensional environment E and a choice of $|e_0\rangle$ and U_{QE}, solving

$$\mathsf{U}_{QE}\,|Q\rangle \otimes |e_0\rangle = \sum_{k=1}^{K} (\Lambda_k\,|Q\rangle) \otimes |e_k\rangle \tag{7}$$

for any pure state $|Q\rangle$ of the principal system Q, and $\{|e_k\rangle\}_{k=1}^{K}$ forming an orthonormal basis of the K-dimensional environment space.

To model by such a Stinespring dilated unitary representation the qubit Pauli noise of Equation (1) defined by $K = 4$ Kraus operators $\Lambda_k = \sqrt{p_k}\sigma_k$, a four-dimensional environment E can be selected, realized by two auxiliary qubits, unitarily interacting via U_{QE} with the principal qubit Q. Yet, as we mentioned earlier, other models for the environment E are possible, with a larger, arbitrarily larger, dimensionality, to equivalently satisfy Equation (6).

To obtain a simulation by a simulating device of the nonunitary quantum operation $\mathcal{N}(\cdot)$, a subsequent step is to materialize with a quantum circuit, constructed from elementary unitary quantum gates, the environment model E and its joint unitary evolution U_{QE} with the principal qubit Q. In the resulting simulating circuit, it is desirable to obtain easy control on the parameters determining $\mathcal{N}(\cdot)$, that is, the set of probabilities (p_0, p_x, p_y, p_z) in the case of the Pauli noises from Equation (1).

For simulating in this fashion the class of Pauli noises from Equation (1), with a two-qubit environment E as envisaged above, if one wants the convenience of a fixed circuit architecture fixing a common U_{QE} for any choice of the four noise parameters (p_0, p_x, p_y, p_z), one displaces in this way the control of (p_0, p_x, p_y, p_z) onto the initial state $|e_0\rangle$ of the two environment qubits. To dispose of enough degrees of freedom, one will usually have to resort to two-qubit entangled states $|e_0\rangle$, for instance under the form

$$|e_0\rangle = \sqrt{p_0}\,|00\rangle + \sqrt{p_x}\,|01\rangle + \sqrt{p_y}\,|10\rangle + \sqrt{p_z}\,|11\rangle\ , \tag{8}$$

that may not be straightforward to prepare with common qubit gates (and presumably restoring a parameter-dependent architecture for the quantum circuit preparing $|e_0\rangle$).

As an alternative in the sequel, we will examine a larger environment model E, relying on three auxiliary qubits instead of two, enabling a simple hardware architecture to implement a fixed U_{QE}, and a control on the four parameters (p_0, p_x, p_y, p_z) of Pauli noise (only three of them are independent) by means of separable initial states for the three environment qubits.

3. A Quantum Circuit for Simulating Pauli Noises

For simulating the qubit Pauli noises from Equation (1), we consider a quantum circuit utilizing three auxiliary qubits and only three elementary quantum gates in the form of a controlled version of each elementary Pauli gate σ_x, σ_y, and σ_z. These three controlled Pauli gates are elementary quantum gates usually readily accessible from the gate libraries of the currently available quantum processors, such as those of [28,29] or others. The three controlled Pauli gates are assembled in the simple pipeline architecture shown in Figure 1.

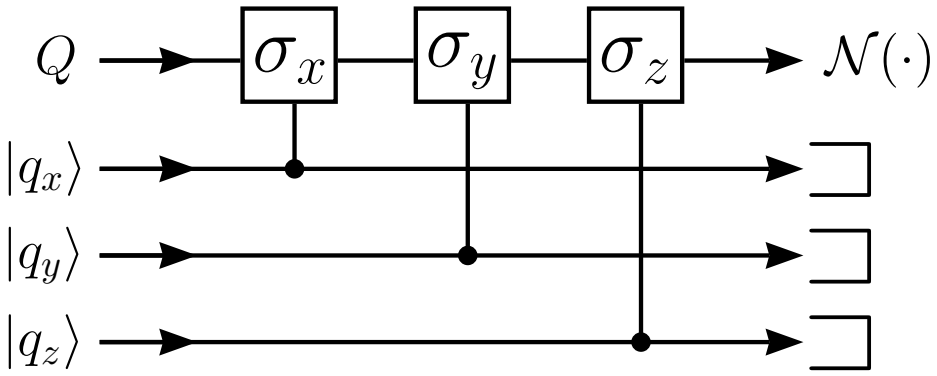

Figure 1. Quantum circuit for simulating a general Pauli noise by realizing the quantum operation $\mathcal{N}(\cdot)$ of Equation (1) on the principal qubit Q. The three-qubit environment E prepared in the pure separable state $|q_x\rangle \otimes |q_y\rangle \otimes |q_z\rangle$ from Equation (9) sets the noise parameters p_k in the presence of a fixed hardware circuit by providing the control qubits to Pauli gates σ_x, σ_y, and σ_z.

Each control qubit to the three Pauli gates in Figure 1 is initialized in the (properly normalized) state of the Hilbert space $\mathcal{H}_2$,

$$|q_k\rangle = \sqrt{1-q_k}\,|0\rangle + \sqrt{q_k}\,|1\rangle \ , \tag{9}$$

for every $k \in \{x, y, z\}$, with each scalar q_k chosen as real in $[0, 1]$. Such a qubit state $|q_k\rangle$ is easily obtained by applying to the initial state $|0\rangle$ the rotation gate

$$\mathsf{R}_y(\xi_k) = \exp\left(-i\,\frac{\xi_k}{2}\sigma_y\right) = \begin{bmatrix} \cos(\xi_k/2) & -\sin(\xi_k/2) \\ \sin(\xi_k/2) & \cos(\xi_k/2) \end{bmatrix} \tag{10}$$

at an angle $\xi_k = 2\arcsin\left(\sqrt{q_k}\right)$, which is also an elementary gate available from the gate libraries of current quantum processors.

Each resulting controlled Pauli gate σ_x, σ_y, and σ_z in Figure 1 acts independently on the principal qubit Q initialized in the normalized state $|Q\rangle$ of the Hilbert space $\mathcal{H}_2$ via a two-qubit unitary evolution formally as in Equation (7) with U_{QE_k}, a two-qubit unitary operator, and taking each time the form

$$\mathsf{U}_{QE_k}\,|Q\rangle \otimes |q_k\rangle = \sqrt{1-q_k}\,|Q\rangle \otimes |0\rangle + \sqrt{q_k}\left(\sigma_k\,|Q\rangle\right) \otimes |1\rangle \ . \tag{11}$$

When the control qubit k is discarded (nonmeasured) in Figure 1 and traced out, formally as in Equation (6), this implements on the qubit density operator $\rho = |Q\rangle\langle Q|$ the one-qubit nonunitary evolution

$$\rho \longmapsto (1-q_k)\rho + q_k\sigma_k\rho\sigma_k^\dagger \ , \tag{12}$$

for every $k \in \{x, y, z\}$.

A more general initialization of the control qubit could be envisaged, with $|q_k\rangle = \alpha_k|0\rangle + \beta_k|1\rangle$ instead of Equation (9), with two complex coordinates (α_k, β_k) satisfying $|\alpha_k|^2 + |\beta_k|^2 = 1$. This would lead to the evolution $\mathsf{U}_{QE_k}|Q\rangle \otimes |q_k\rangle = \alpha_k|Q\rangle \otimes |0\rangle + \beta_k(\sigma_k|Q\rangle) \otimes |1\rangle$ instead of Equation (11). Then, when tracing out the control qubit as conducted for obtaining Equation (12), we would obtain $\rho \mapsto |\alpha_k|^2\rho + |\beta_k|^2\sigma_k\rho\sigma_k^\dagger$ instead of Equation (12). We therefore observe that no additional flexibility would be gained with two complex coordinates (α_k, β_k) since only the squared moduli $|\alpha_k|^2$ and $|\beta_k|^2$ affect the noise model, and this control is already fully obtained with the initialization of Equation (9) with real coordinates and the rotation gate R_y of Equation (10).

For every given $k \in \{x, y, z\}$, the evolution of Equation (12) can be described as a matrix transformation of the qubit Bloch vector, similar to Equation (2), yet with only two nonzero probabilities, formally $q_k \equiv p_k$ and $1 - q_k \equiv p_0$. Three such matrix transformations are cascaded when the three control qubits acting independently in the circuit of Figure 1 are successively traced out while tracing out the environment E. It results that, when the three control qubits are discarded (nonmeasured), the circuit of Figure 1 implements on the principal qubit Q with input Bloch vector $\vec{r}$ the overall transformation in Bloch representation

$$\vec{r} \longmapsto \vec{r}\,' = \begin{bmatrix} 1-2q_z & 0 & 0 \\ 0 & 1-2q_z & 0 \\ 0 & 0 & 1 \end{bmatrix} \begin{bmatrix} 1-2q_y & 0 & 0 \\ 0 & 1 & 0 \\ 0 & 0 & 1-2q_y \end{bmatrix} \begin{bmatrix} 1 & 0 & 0 \\ 0 & 1-2q_x & 0 \\ 0 & 0 & 1-2q_x \end{bmatrix} \vec{r}\,, \tag{13}$$

which is also

$$\vec{r} \longmapsto \vec{r}\,' = \begin{bmatrix} (1-2q_y)(1-2q_z) & 0 & 0 \\ 0 & (1-2q_x)(1-2q_z) & 0 \\ 0 & 0 & (1-2q_x)(1-2q_y) \end{bmatrix} \vec{r}\,. \tag{14}$$

Incidently, since in Equation (13) the products of the three diagonal matrices commute, the three controlled Pauli gates can be cascaded in any order in the pipeline of Figure 1 without changing the circuit behavior.

We want the transformation of Equation (14) to implement the Pauli noise transformation of Equation (2). By Equations (3)–(5), this requires the three control parameters (q_x, q_y, q_z) of the circuit in Figure 1 to satisfy the nonlinear algebraic system

$$\begin{cases} q_y + q_z - 2q_yq_z = p_y + p_z\,, & (15) \\ q_x + q_z - 2q_xq_z = p_x + p_z\,, & (16) \\ q_x + q_y - 2q_xq_y = p_x + p_y\,. & (17) \end{cases}$$

The nonlinear system of Equations (15)–(17) can be solved explicitly as

$$\begin{cases} q_x = \dfrac{1}{2}\left(1 \pm \dfrac{\sqrt{\Delta}}{1-2(p_y+p_z)}\right) = \dfrac{1}{2}\left(1 \pm \mathrm{sign}(a_x)\sqrt{\dfrac{a_ya_z}{a_x}}\right), & (18) \\ q_y = \dfrac{1}{2}\left(1 \pm \dfrac{\sqrt{\Delta}}{1-2(p_x+p_z)}\right) = \dfrac{1}{2}\left(1 \pm \mathrm{sign}(a_y)\sqrt{\dfrac{a_xa_z}{a_y}}\right), & (19) \\ q_z = \dfrac{1}{2}\left(1 \pm \dfrac{\sqrt{\Delta}}{1-2(p_x+p_y)}\right) = \dfrac{1}{2}\left(1 \pm \mathrm{sign}(a_z)\sqrt{\dfrac{a_xa_y}{a_z}}\right), & (20) \end{cases}$$

with the discriminant

$$\Delta = \left[1-2(p_x+p_y)\right]\left[1-2(p_x+p_z)\right]\left[1-2(p_y+p_z)\right] = a_xa_ya_z\,, \tag{21}$$

to define two feasible sets of solutions $(q_x, q_y, q_z)_+$ and $(q_x, q_y, q_z)_-$ according to the $\pm$ sign chosen in Equations (18)–(20). However, every solution (q_x, q_y, q_z) from Equations (18)–(20) solving the system of Equations (15)–(17) does not necessarily represent an admissible solu-

tion to our noise simulation problem. For instance, with three real a_k in $[-1,1]$ as delivered by Equations (3)–(5), complex numbers (q_x, q_y, q_z) can ensue in Equations (18)–(20) when a negative discriminant Δ occurs in Equation (21) that indeed solves Equations (15)–(17) but is not admissible for our noise simulation problem. Our noise simulation problem requires each solution q_k provided in Equations (18)–(20) to be real and in $[0,1]$. This would be no different if we had envisaged as before the more general control $|q_k\rangle = \alpha_k |0\rangle + \beta_k |1\rangle$ instead of Equation (9), which would have provided $\rho \mapsto |\alpha_k|^2 \rho + |\beta_k|^2 \sigma_k \rho \sigma_k^\dagger$ instead of Equation (12), with $|\beta_k|^2$ in place of q_k, which is equally constrained to remain in $[0,1]$ for an admissible solution. We therefore have an admissible solution to our noise simulation problem if and only if each q_k provided in Equations (18)–(20) is real and in $[0,1]$. In terms of the three variables

$$\begin{cases} s_x = \dfrac{a_y a_z}{a_x} , & (22) \\ s_y = \dfrac{a_x a_z}{a_y} , & (23) \\ s_z = \dfrac{a_x a_y}{a_z} , & (24) \end{cases}$$

an admissible solution in Equations (18)–(20) for our noise simulation problem requires each s_k to be in $[0,1]$ for $k = x, y, z$. For any valid set of probabilities (p_0, p_x, p_y, p_z), each contraction factor a_k in Equations (3)–(5) varies in $[-1,1]$; as a result, the three variables s_k in Equations (22)–(24) can vary in $]-\infty, +\infty[$, and only when these three variables s_k lie in $[0,1]$ can the corresponding Pauli noise be simulated by the circuit of Figure 1. This establishes the essential condition for simulability, which we state as

Theorem 1. *A given set of probabilities (p_x, p_y, p_z) defining with $p_0 = 1 - p_x - p_y - p_z$ a valid Pauli noise can be simulated by the circuit of Figure 1 with a setting (q_x, q_y, q_z) of three real parameters in $[0,1]$ provided in Equations (18)–(20) if and only if all three variables s_k in Equations (22)–(24) are in $[0,1]$.*

Proof of Theorem 1. For $k = x, y, z$, each q_k in Equations (18)–(20) is $q_k = \left(1 \pm \text{sign}(a_k) \sqrt{s_k}\right)/2$. The square root $\sqrt{s_k}$ is real if and only if $s_k \geq 0$. The resulting q_k is in $[0,1]$ if and only if each $s_k \geq 0$ is no larger than 1. Therefore, q_k is in $[0,1]$ if and only if s_k is in $[0,1]$ for $k = x, y, z$, which completes the proof. □

The Pauli noise configurations (p_x, p_y, p_z) that satisfy the condition of Theorem 1 can be associated with a feasible set of control parameters (q_x, q_y, q_z) in Equations (15)–(17) and can therefore be simulated by the quantum circuit of Figure 1. Conversely, when a noise configuration (p_x, p_y, p_z) does not satisfy the condition of Theorem 1, i.e., when at least one variable s_k from Equations (22)–(24) is not in $[0,1]$, this configuration cannot be simulated by the circuit of Figure 1 because the corresponding variable q_k is not in $[0,1]$ and no suitable control $|q_k\rangle$ in Equation (9) can be physically realized for the circuit. The simulable Pauli noise configurations (p_x, p_y, p_z) form a nontrivial set, which, in addition to the algebraic characterization of Theorem 1, can be graphically visualized by means of the illustrations provided in Figures 2–6.

To begin with, Figure 2 displays, in the three-dimensional space $\mathbb{R}^3$, the probability configurations (p_x, p_y, p_z) defining a valid quantum Pauli noise in Equation (1) by satisfying $0 \leq p_x + p_y + p_z \leq 1$.

As visible in Figure 2, the acceptable configurations (p_x, p_y, p_z) defining a valid quantum Pauli noise form a solid tetrahedron in $\mathbb{R}^3$. In this tetrahedron, the valid Pauli noise configurations (p_x, p_y, p_z) that can be simulated by the quantum circuit of Figure 1 are those that satisfy Theorem 1, i.e., those having all three variables s_k of Equations (22)–(24) in $[0,1]$. To visualize these Pauli noise configurations that can be simulated by the circuit of Figure 1, the tetrahedron of valid Pauli noise configurations of Figure 2 is sliced in Figures 3 and 4 along the axis of p_x. In each slice at given probability p_x, in the plane (p_y, p_z), each configuration (p_x, p_y, p_z) that can be simulated is marked in green, while it is marked in red when it

cannot. In practice, in each slice in Figures 3 and 4, a uniform Monte Carlo sampling of 10^5 configurations of (p_y, p_z) are obtained and tested according to Theorem 1 to be marked by a green or red pixel. As can be observed from Equations (18)–(20) and Equations (22)–(24), the criterion represented in Figures 3 and 4 is symmetric or invariant in the exchange of the noise probabilities p_x, p_y, and p_z, so these figures will have the same appearance if instead of p_x we fix p_y or p_z and vary the other two probabilities.

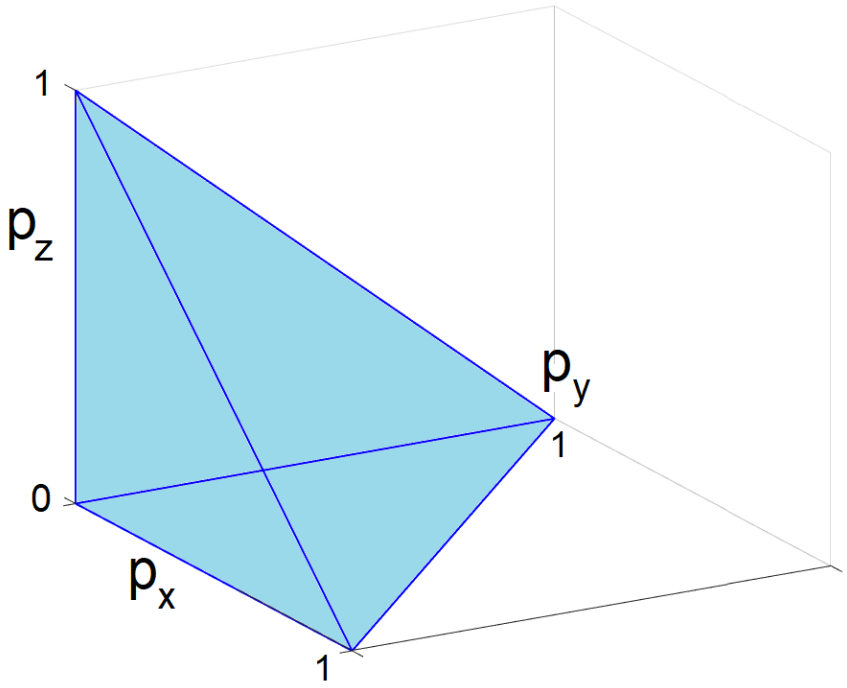

Figure 2. In the three-dimensional space $\mathbb{R}^3$, the tetrahedron in blue has its four vertices at points $(0,0,0)$, $(1,0,0)$, $(0,1,0)$, and $(0,0,1)$, and its interior (including its frontier) represents all the probability configurations (p_x, p_y, p_z) satisfying $0 \leq p_x + p_y + p_z \leq 1$ and defining a valid quantum Pauli noise in Equation (1).

For the range $0 \leq p_x < 0.5$, Figure 3 shows slices of the tetrahedron of Figure 2 in the planar domain $(p_y, p_z) \in [0,1] \times [0,1]$.

Figure 3 illustrates the nontrivial structure of the simulable and nonsimulable noise configurations resulting from the algebraic nonlinear criterion involved in Theorem 1 and coupling the variables (p_x, p_y, p_z). We observe in particular a nonmonotonic evolution of the surface (the amount) of simulable configurations, which starts to increase and then decreases across the slices as p_x grows from 0 to 0.5 in Figure 3.

Next, for the range $0.5 \leq p_x \leq 1$, Figure 4 shows slices of the tetrahedron of Figure 2 in the planar domain $(p_y, p_z) \in [0, 0.5] \times [0, 0.5]$ since, from the normalization condition when the probability $p_x \geq 0.5$, the probabilities p_y and p_z are necessarily in $[0, 0.5]$.

Figure 4 further illustrates the nontrivial structure of the simulable and nonsimulable noise configurations, as ruled by the algebraic criterion of Theorem 1. In this range, $0.5 \leq p_x \leq 1$, we rather observe a monotonic decay of the surface (the amount) of simulable configurations across the slices as p_x increases in Figure 4 and while reaching the tip of the tetrahedron of valid Pauli noise configurations in Figure 2.

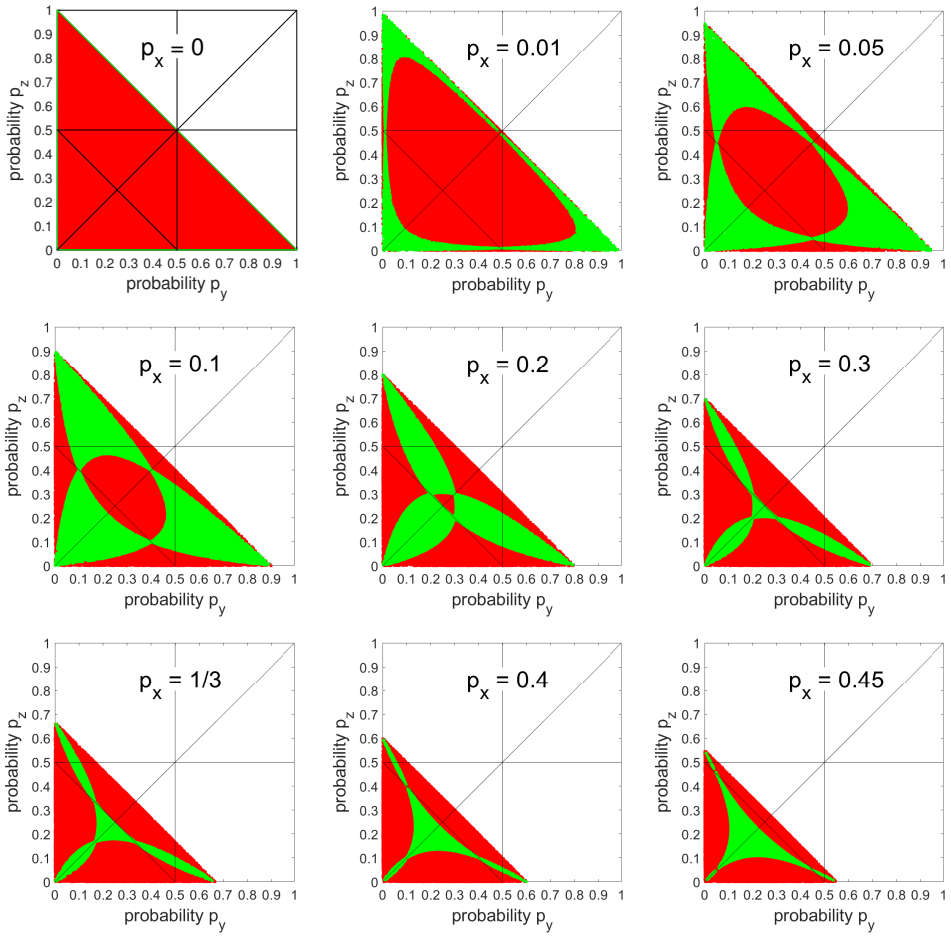

Figure 3. At fixed probabilities p_x, in the plane (p_y, p_z), the Pauli noise configurations that can be simulated by the circuit of Figure 1 are marked in green, and the configurations that cannot be simulated are in red.

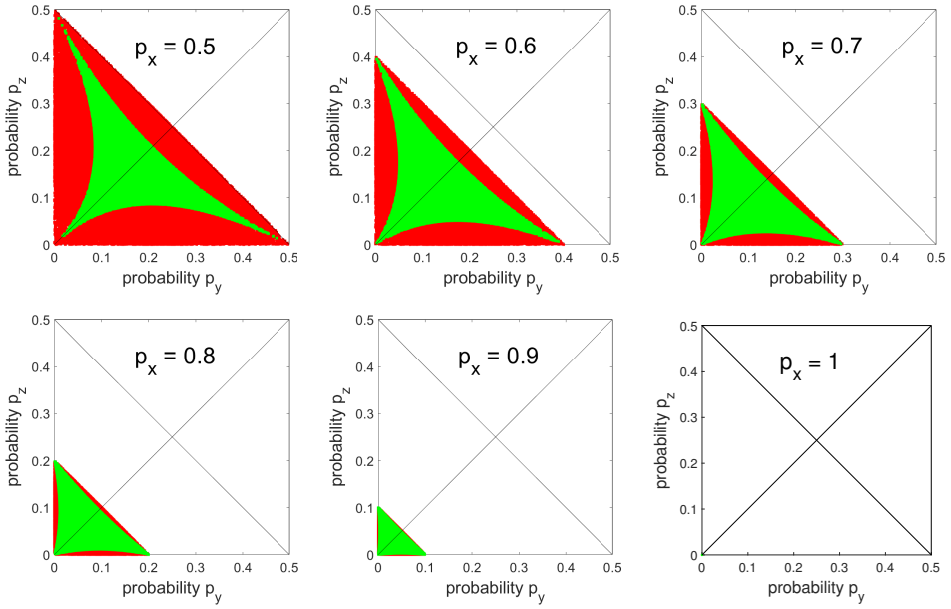

Figure 4. At fixed probabilities p_x, in the plane (p_y, p_z), the Pauli noise configurations that can be simulated by the circuit of Figure 1 are marked in green, and the configurations that cannot be simulated are in red.

Furthermore, it results from Theorem 1 that, with the quantum circuit of Figure 1, we have the following possibilities for simulating important Pauli noises:

- The bit-flip noise with $(p_0, p_x, p_y, p_z) = (1 - p_x, p_x, 0, 0)$ can be obtained with $(q_x = p_x, q_y = 0, q_z = 0)$ (alternatively, $(q_x = 1 - p_x, q_y = 1, q_z = 1)$ is also feasible).
- The phase-flip noise with $(p_0, p_x, p_y, p_z) = (1 - p_z, 0, 0, p_z)$ can be obtained with $(q_x = 0, q_y = 0, q_z = p_z)$.
- The bit-phase-flip noise with $(p_0, p_x, p_y, p_z) = (1 - p_y, 0, p_y, 0)$ can be obtained with $(q_x = 0, q_y = p_y, q_z = 0)$.
- The depolarizing noise with $(p_0, p_x, p_y, p_z) = (1 - p, p/3, p/3, p/3)$ can be obtained with

$$q_x = q_y = q_z = \frac{1}{2}\left(1 \pm \sqrt{1 - \frac{4}{3}p}\right), \tag{25}$$

  when $p \in [0, 3/4]$; otherwise, when $p > 3/4$, the corresponding Pauli noise can no longer be simulated by the circuit of Figure 1. The limit $p = 3/4$ corresponds to the depolarizing noise for three vanishing contraction factors $a_x = a_y = a_z = 0$ in Equations (3)–(5) when the input state ρ is transformed by the noise into the maximally mixed output state $I_2/2$. When the noise parameter p continues to grow above $3/4$, up to $p = 1$, three negative contraction factors $a_x = a_y = a_z = 1 - 4p/3 < 0$ ensue in Equations (3)–(5), with a noisy qubit state that would tend to recover from the maximally mixed state $I_2/2$ into a somehow less noisy (less mixed) state. Due to this nonmonotonic evolution, the regime of $p > 3/4$, although formally acceptable in the depolarizing noise model, comes with a less natural physical plausibility of being relevant or observable in practice. Reversing the viewpoint, we could say that, when a depolarizing noise is introduced to model the interaction of a qubit with an unobserved physical environment, and when this environment takes the form of the circuit of Figure 1, only depolarizing noise characterized by a parameter $p \in [0, 3/4]$ arises. Such depolarizing noise exhibits in Equation (2) a uniform contraction factor $a_x = a_y = a_z = 1 - 4p/3 \in [0, 1]$, describing a monotonic degradation, from a vanishing alteration of the qubit state at $p = 0$ with no noise and $a_x = a_y = a_z = 1$, up to an extreme alteration at $p = 3/4$ when $a_x = a_y = a_z = 0$ and the qubit state is forced into the maximally mixed state $I_2/2$. The physics of the interaction with the environment of the circuit of Figure 1 give rise only to this range of noise action.

The situation in the three-dimensional probability space (p_x, p_y, p_z) of these four important Pauli noises is represented graphically in Figure 5.

Three other remarkable subsets of Pauli noises that can be simulated by the circuit of Figure 1 are those where only two nontrivial Pauli operators act, and they are represented in Figure 6. One such subset corresponds to the situation with the probabilities $p_0 = p_x = 0$ and $p_y = 1 - p_z$; this leads in Equations (3)–(5) to the contraction factors $a_x = -1$, $a_y = -a_z = p_y - p_z$, simulable in Equations (18)–(20) with the control signals $(q_x, q_y, q_z) = (p_y, 0, 1)$ or $(q_x, q_y, q_z) = (1 - p_y, 1, 0)$. The two other subsets of Figure 6 follow by symmetry.

As expressed by Figures 5 and 6, all six edges of the tetrahedron in Figure 2 of valid Pauli noise configurations are simulable by the quantum circuit of Figure 1, corresponding to Pauli noises where only a pair of trivial or nontrivial Pauli operators are acting. In addition, (infinitely) many more Pauli noise configurations are simulable from the interior of the tetrahedron of Figure 2, as expressed by Figures 3 and 4.

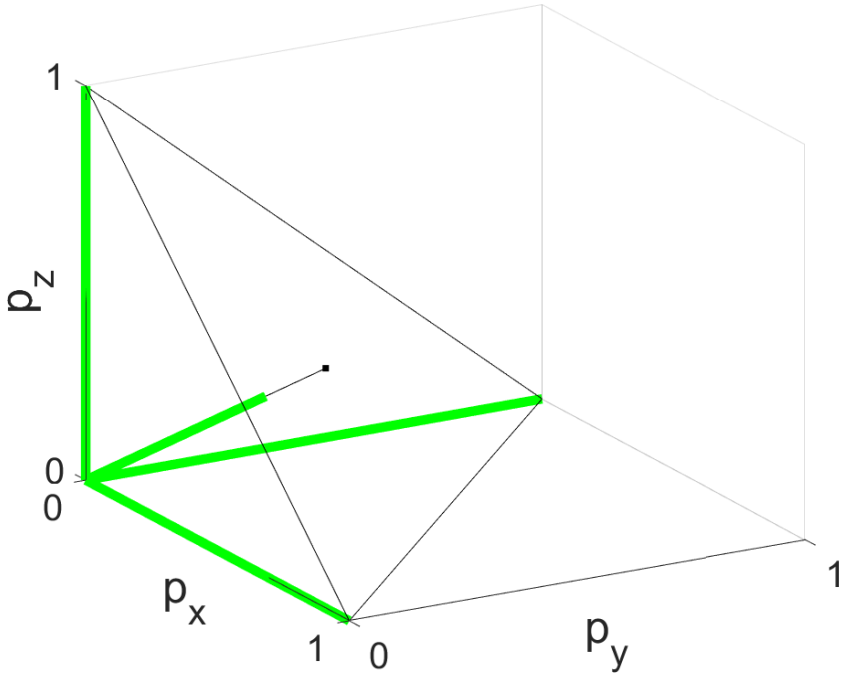

Figure 5. In the three-dimensional probability space (p_x, p_y, p_z), the four green lines represent four important Pauli noises simulable with the quantum circuit of Figure 1. Bit-flip, phase-flip, and bit-phase-flip noises are, respectively, along the p_x, p_z, and p_y axes. The depolarizing noise with $(p_x, p_y, p_z) = (p/3, p/3, p/3)$ for $p \in [0, 3/4]$ stands along the main diagonal.

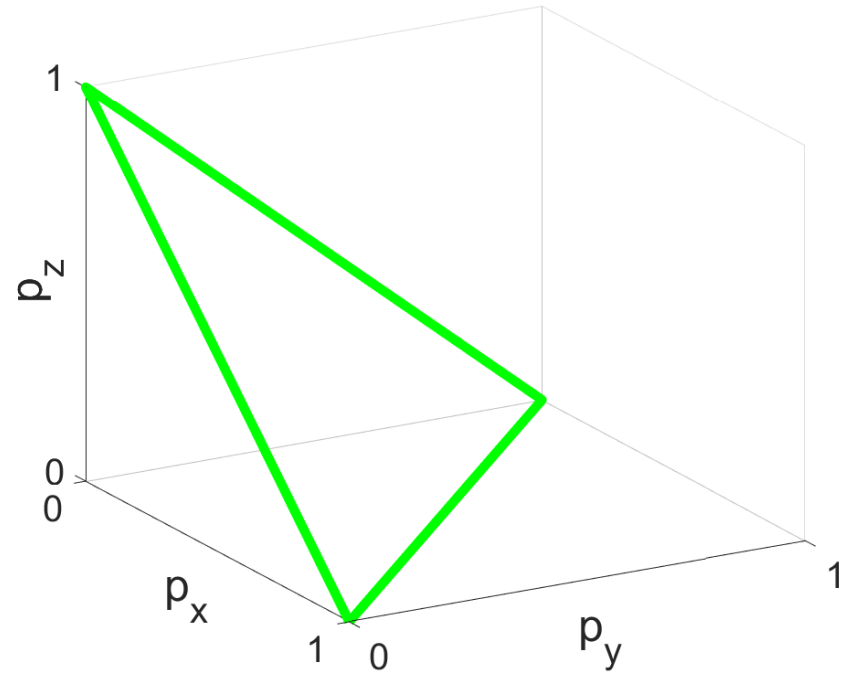

Figure 6. In the three-dimensional probability space (p_x, p_y, p_z), the three green lines represent three subsets of Pauli noises simulable with the quantum circuit of Figure 1, where only two nontrivial Pauli operators act, and defined by the parameters (p_0, p_x, p_y, p_z), respectively, being $(0, 0, p_y, 1 - p_y)$, $(0, 1 - p_z, 0, p_z)$, and $(0, p_x, 1 - p_x, 0)$.

4. Conclusions

For Pauli noise simulation, the quantum circuit of Figure 1 uses only three Pauli gates in their controlled version, which are elementary quantum gates usually readily accessible from the gate libraries of currently available quantum processors, such as those of [28,29] or others under development and constant progress. Standard quantum processors are primarily devised for implementing *unitary* evolutions for quantum algorithms of quantum computation. By contrast, circuit models for controlled simulation of quantum noise or decoherence, as with the circuit examined here, enable implementing *nonunitary* evolutions with these quantum processors. This enlarges the class of quantum scenarios that can be addressed with these processors, especially in the direction of realistic processes of quantum signal and information processing in the presence of quantum noise.

The quantum circuit of Figure 1 offers the possibility to constitute experimental testbeds or simulation platforms where quantum Pauli noise can be applied to qubits in controlled conditions. The impact of Pauli noise can then be analyzed in various scenarios, for instance on signaling qubits for communication or for cryptographic key distribution over a noisy quantum channel, or on probe qubits for noisy quantum metrology, or in other tasks of interest with noisy qubits, as mentioned in the Introduction. Pauli noise can be applied and simulated on multiple entangled qubits in a regime often relevant in practice where the noise acts independently on distinct qubits. Independent action of Pauli noise is intrinsic to its definition conveyed by Equation (1) as it randomly applies the four qubit Pauli operators independently on each distinct qubit. Accordingly, the simulation circuit of Figure 1 reproduces this intrinsic property of Pauli noise when an independent copy of the circuit is used for each principal (entangled or separable) qubit. This provides us the possibility, with an experimental simulation platform based on the circuit of Figure 1, to study the impact of Pauli noise on multiple entangled qubits. In this respect, in many situations with noise on entangled qubits, the optimal configurations to maximize the signal processing performance are not fully characterized, for instance to achieve the capacity of a noisy communication channel or minimize the estimation errors in noisy metrology, and can be studied in simulation. Alternatively, in the circuit of Figure 1, the same control qubits could be used several times, according to different patterns, to control the noise on several distinct principal qubits instead of three independent control qubits per principal qubit. This would induce specific correlations between the noise realizations on multiple qubits whenever they are assumed realistic for the noise in specific contexts, thus extending the capabilities of a simulation platform.

The quantum circuit of Figure 1, as a model for simulating Pauli noises, is convenient in terms of its fixed and simple architecture and the ease in the control on the noise parameters without changing the hardware architecture. Each of the three independent parameters (p_x, p_y, p_z) defining Pauli noise are programmed by means of the state of an independent auxiliary qubit acting on the fixed hardware architecture. The circuit incorporates enough flexibility to simulate essential Pauli noises relevant to the qubit, as illustrated in Figure 5, along with an infinite subset of other Pauli noises, also with the same fixed and, so to speak, programmable hardware architecture. The limitation of the quantum circuit of Figure 1 essentially comes from the fact that the actions of the three controlled Pauli gates are cascaded, and each acts to contract the qubit Bloch vector in two directions of $\mathbb{R}^3$, as expressed by Equation (13). These contractions cannot always be combined or decoupled so as to produce three specific contractions along the three directions of $\mathbb{R}^3$, as may be demanded by some acceptable Pauli noises in Equation (2). To gain additional flexibility, one could envisage replacing the three Pauli gates, σ_x, σ_y, and σ_z in the circuit of Figure 1, by three rotation gates, $\mathsf{R_x} = \exp\left(-i\xi_x\sigma_x/2\right)$, $\mathsf{R_y} = \exp\left(-i\xi_y\sigma_y/2\right)$, and $\mathsf{R_z} = \exp\left(-i\xi_z\sigma_z/2\right)$, benefiting from extra degrees of freedom in the three angles ξ_x, ξ_y, and ξ_z. In its version controlled by $|q_k\rangle$ of Equation (9), each rotation gate $\mathsf{R_k}$ would realize on the Bloch vector $\vec{r}$ the transformation $\vec{r} \mapsto (1-q_k)\vec{r} + q_k\mathsf{R_k}\vec{r}$ for each $k = x, y, z$, which in general is not a diagonal transformation in $\mathbb{R}^3$, while each Pauli gate σ_k realizes a diagonal transformation in $\mathbb{R}^3$, provided by each of the three diagonal matrices appearing in

Equation (13), for $k = x, y, z$. In the cascade of Figure 1, while the three Pauli gates together realize the diagonal transformation of Equation (14) to simulate the diagonal matrix of Equation (2) defining Pauli noise, the three rotation gates together would instead realize a generally nondiagonal transformation in $\mathbb{R}^3$. The three angles of the three rotation gates could then be exploited so as to make this transformation diagonal. By explicitly expressing this transformation matrix in $\mathbb{R}^3$, it is found that its diagonalization is feasible (nontrivially) only with the rotation angles $\xi_x = \xi_y = \xi_z = \pi$, where the three rotation gates all match the Pauli gates with $\mathsf{R_x} \equiv -i\sigma_x$, $\mathsf{R_y} \equiv -i\sigma_y$, and $\mathsf{R_z} \equiv -i\sigma_z$. Consequently, for Pauli noise simulation, no additional capability can be gained with three rotation gates, $\mathsf{R_x}$, $\mathsf{R_y}$, and $\mathsf{R_z}$, in place of the three Pauli gates used in the circuit of Figure 1. Alternatively, other quantum circuits could still in principle be devised for simulation of Pauli noises, each expected to come with its inherent properties and limitations, including the possibility or not to have a fixed architecture to simulate a whole range of noise models, and together offering different trade-offs between capabilities, simplicity of implementation, flexibility, and control. Such tools, like the circuit investigated here, are useful to construct experimental simulation platforms for various information processing tasks with controlled quantum noise so as to contribute to the design and development of quantum methodologies and technologies capable of better coping with quantum noise and decoherence.

Funding: This research received no external funding.

Data Availability Statement: The original contributions presented in the study are included in the article, further inquiries can be directed to the corresponding author.

Conflicts of Interest: The author declares no conflicts of interest.

References

1. Schleich, W.P.; Ranade, K.S.; Anton, C.; Arndt, M.; Aspelmeyer, M.; Bayer, M.; Berg, G.; Calarco, T.; Fuchs, H.; Giacobino, E.; et al. Quantum technology: From research to application. *Appl. Phys. B* **2016**, *122*, 130
2. Preskill, J. Quantum computing in the NISQ (Noisy Intermediate-Scale Quantum) era and beyond. *Quantum* **2018**, *2*, 79. [CrossRef]
3. Xin, K.; Lai, M.; Lv, F.; Guo, K.; Pang, Z.; Xu, C.; Zhang, G.; Wang, W.; Li, M. A cryo-CMOS, low-power, low-noise, phase-locked loop design for quantum computers. *Electronics* **2023**, *12*, 3237. [CrossRef]
4. Wilde, M.M. *Quantum Information Theory*; Cambridge University Press: Cambridge, UK, 2017.
5. Gyongyosi, L.; Imre, S.; Nguyen, H.V. A survey on quantum channel capacities. *IEEE Commun. Surv. Tutorials* **2018**, *20*, 1149–1205. [CrossRef]
6. Gisin, N.; Ribordy, G.; Tittel, W.; Zbinden, H. Quantum cryptography. *Rev. Mod. Phys.* **2002**, *74*, 145–195. [CrossRef]
7. Pirandola, S.; Andersen, U.L.; Banchi, L.; Berta, M.; Bunandar, D.; Colbeck, R.; Englund, D.; Gehring, T.; Lupo, C.; Ottaviani, C.; et al. Advances in quantum cryptography. *Adv. Opt. Photonics* **2020**, *12*, 1012–1236. [CrossRef]
8. Giovannetti, V.; Lloyd, S.; Maccone, L. Advances in quantum metrology. *Nat. Photonics* **2011**, *5*, 222–229. [CrossRef]
9. Shaji, A.; Caves, C.M. Qubit metrology and decoherence. *Phys. Rev. A* **2007**, *76*, 032111. [CrossRef]
10. Paris, M.G.A.; Řeháček , J. (Eds.) *Quantum State Estimation*; Lecture Notes in Physics; Springer: Berlin, Germany, 2004; Volume 649.
11. Koch, C.P.; Boscain, U.; Calarco, T.; Dirr, G.; Filipp, S.; Glaser, S.J.; Kosloff, R.; Montangero, S.; Schulte-Herbrüggen, T.; Sugny, D.; et al. Quantum optimal control in quantum technologies. Strategic report on current status, visions and goals for 367 research in Europe. *EPJ Quantum Technol.* **2022**, *9*, 19. [CrossRef]
12. Dunjko, V.; Briegel, H.J. Machine learning & artificial intelligence in the quantum domain: A review of recent progress. *Rep. Prog. Phys.* **2018**, *81*, 074001.
13. Cerezo, M.; Verdon, G.; Huang, H.Y.; Cincio, L.; Coles, P.J. Challenges and opportunities in quantum machine learning. *Nat. Comput. Sci.* **2022**, *2*, 567–576. [CrossRef]
14. Costa, N.F.; Omar, Y.; Sultanov, A.; Paraoanu, G.S. Benchmarking machine learning algorithms for adaptive quantum phase estimation with noisy intermediate-scale quantum sensors. *EPJ Quantum Technol.* **2021**, *8*, 16. [CrossRef]
15. Ting, J.J.L. Stochastic resonance for quantum channels. *Phys. Rev. E* **1999**, *59*, 2801–2803. [CrossRef]
16. Bowen, G.; Mancini, S. Stochastic resonance effects in quantum channels. *Phys. Lett. A* **2006**, *352*, 272–275. [CrossRef]
17. Gillard, N.; Belin, E.; Chapeau-Blondeau, F. Stochastic resonance with unital quantum noise. *Fluct. Noise Lett.* **2019**, *18*, 1950015. [CrossRef]
18. Gaitan, F. *Quantum Error Correction and Fault Tolerant Quantum Computing*; CRC Press: Boca Raton, FL, USA, 2008.
19. Djordjevic, I.B. *Quantum Information Processing, Quantum Computing, and Quantum Error Correction: An Engineering Approach*; Academic Press: New York, NY, USA, 2021.

20. Nielsen, M.A.; Chuang, I.L. *Quantum Computation and Quantum Information*; Cambridge University Press: Cambridge, UK, 2000.
21. Chapeau-Blondeau, F. Modeling and simulation of a quantum thermal noise on the qubit. *Fluct. Noise Lett.* **2022**, *21*, 2250060. [CrossRef]
22. Chapeau-Blondeau, F. Optimization of quantum states for signaling across an arbitrary qubit noise channel with minimum-error detection. *IEEE Trans. Inf. Theory* **2015**, *61*, 4500–4510. [CrossRef]
23. Chiuri, A.; Rosati, V.; Vallone, G.; Pádua, S.; Imai, H.; Giacomini, S.; Macchiavello, C.; Mataloni, P. Experimental realization of optimal noise estimation for a general Pauli channel. *Phys. Rev. Lett.* **2011**, *107*, 253602. [CrossRef]
24. Collins, D. Mixed-state Pauli-channel parameter estimation. *Phys. Rev. A* **2013**, *87*, 032301. [CrossRef]
25. Chapeau-Blondeau, F. Optimized probing states for qubit phase estimation with general quantum noise. *Phys. Rev. A* **2015**, *91*, 052310. [CrossRef]
26. Ting, J.J.L. Noise effects on one-Pauli channel. *Eur. Phys. J. B* **2000**, *13*, 527–530.
27. Chen, S.; Liu, Y.; Otten, M.; Seif, A.; Fefferman, B.; Jiang, L. The learnability of Pauli noise. *Nat. Commun.* **2023**, *14*, 52. [CrossRef] [PubMed]
28. Chang, W.-L.; Vasilakos, A.V. *Fundamentals of Quantum Programming in IBM's Quantum Computers*; Springer: Cham, Switzerland, 2021.
29. Khan, A. *Quantum Computing Experimentation with Amazon Braket*; Packt Publishing: Birmingham, UK, 2022.